Ph.D. Thesis Proposal
Measurement of the Coulomb quadrupole amplitude in the $\gamma^* p \rightarrow \Delta(1232)$ reaction in the low momentum transfer region

David Anez
Dalhousie University

April 20, 2010

Abstract

Experiment E08-010 in Hall A at Jefferson Lab proposes to measure the Coulomb quadrupole transition amplitude of the pion electroproduction reaction with energies near the Δ resonance and a low momentum transfer between the electron and proton. The results of this experiment will help expand knowledge about the CMR at low Q^2, which in turn will increase the world's knowledge about nucleon deformation and pion cloud influence in this region.

1 Introduction

The main goal of this research experiment is to measure the Coulomb, or scalar, quadrupole transition amplitude for the pion electroproduction reaction in the Δ(1232) resonance region with low momentum transfer between the proton and the electron.

Many experiments in the last ten years have conclusively proven that the proton is not spherical, but instead has some sort of "deformation", as evidenced by non-spherical components in the nucleon wave function [1, and references therein]. These deformations may originate from several possible sources, such as the non-central color hyperfine interaction between constituent quarks at short-range or an asymmetric coupling of a pion cloud to the quark core at long-range.

Experiment E08-010, which will be performed at Jefferson Lab in April of 2011, will take measurements of the $p(e,e'p)\pi^0$ reaction using the two high resolution spectrometers (HRS) in Hall A at the facility. From these measurements, the ratio of the Coulomb quadrupole amplitude to the magnetic dipole amplitude (CMR) will be extracted for three different momentum transfer values. This data will help bridge the gap in the world data in the very low momentum transfer region as well as validate the world data in a region of low momentum transfer, overlapping existing results. It will also help constrain theoretical models concerning the "shape" of the nucleon, and help explore the source of the nucleon's "deformation".

2 Physics Motivation via the Constituent Quark Model

Prior to the discovery of quarks and the development of quantum chromodynamics (QCD), it was believed that the proton and neutron were fundamental particles. Though they have since been demoted to composite particles made of still-smaller – and hopefully fundamental – quarks, there was initially no reason to believe they were not spherical.

It was not until 1979 that the idea of a non-spherical proton (or neutron or nucleon) was first developed [2], in which a non-spherical component to the particle's wave function results in a "deformation" to the particle's "shape".

Quotation marks are used when referring to "deformation" and "shape", since there is no unique quantum mechanical definition for these classical terms. However, since these terms are used in the literature to discuss these topics, they will be used here as well.

Using the constituent quark model (CQM), in which the nucleon is composed of three "heavy" quarks, where the mass of each quark is one-third the mass of the nucleon, the general form of the nucleon's wave function can be determined by examining the quarks' spin-orbit coupling.

Each of the three quarks has an intrinsic spin angular momentum, S, of $^1\!/_2$. These spins can combine to form a total spin of $^1\!/_2$ or $^3\!/_2$. If there is no orbital angular momentum, L, this total spin becomes the composite particle's total angular momentum, J, with the $^1\!/_2$ corresponding to the nucleon and the $^3\!/_2$ corresponding to the Δ.

However, L need not be zero. Due to parity conservation, $L = 2$ is also a possibility. This results in additional combinations of spin and orbital angular momenta that can also result in the overall spin of the nucleon or Δ.

A nucleon wave function can then be constructed as a linear combination of the two coupling possibilities, with the $L = 0$ term being the spherical component and the $L = 2$ term being the non-spherical component [3].

$$\left|N(939)\right\rangle = a_S\left|\left(S=\tfrac{1}{2}, L=0\right)J^\pi = \tfrac{1}{2}^+\right\rangle + a_D\left|\left(S=\tfrac{3}{2}, L=2\right)J^\pi = \tfrac{1}{2}^+\right\rangle$$

The Δ(1232) wave function can be constructed in a similar manner.

$$\left|\Delta(1232)\right\rangle = b_S\left|\left(S=\tfrac{3}{2}, L=0\right)J^\pi = \tfrac{3}{2}^+\right\rangle + b_D\left|\left(S=\tfrac{1}{2}, L=2\right)J^\pi = \tfrac{3}{2}^+\right\rangle$$

A natural way to measure an object's deviation from spherical is to measure its quadrupole moment. Unfortunately, the quadrupole moment of the nucleon cannot be measured directly, since it is zero by definition. Instead, the quadrupole moment of the nucleon's transition to a higher spin particle, such as the Δ(1232), is measured.

The proton can be excited to a Δ(1232) electromagnetically with photons, either real or virtual (such as via electrons). Due to angular momentum coupling restrictions, only three electromagnetic transitions can excite a proton to a Δ: the magnetic dipole ($M1$), the electric quadrupole ($E2$), and the scalar or Coulomb quadrupole ($C2$).

In the CQM, the $L = 0$ component of the nucleon's wave function can be visualized with all three quarks in an *s*-state energy level, with two quarks spin up and one quark spin down, resulting in the total spin of $^1/_2$. Likewise, the $L = 0$ component of the Δ's wave function has all three quarks in the *s*-state energy level with spins in the same direction, resulting in the total spin of $^3/_2$, as visualized in Figure 1 [3].

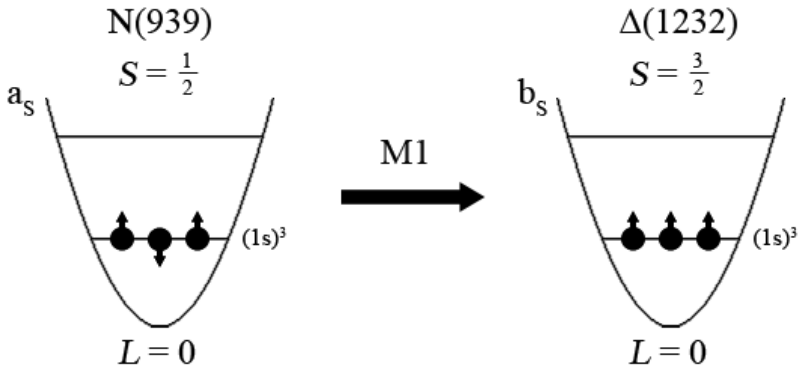

Figure 1: Constituent Quark Model of the nucleon and Δ, with *M*1 transition.
Figure taken from Reference [3].

The magnetic dipole transition, then, is simply a spin flip of the nucleon's odd quark, leaving all three quarks with spins in the same direction, resulting in a Δ(1232). This is the dominant transition observed between the nucleon and the Δ [4].

The $L = 2$ components, on the other hand, can be visualized as one of the quarks being elevated to a *d*-state energy level. This means that the two quadrupole transitions can be thought of as quark transitions between the *s*-state and *d*-state energy levels without a spin flip, as visualized in Figure 2 on the next page [3]. These transitions are known as the color hyperfine interaction [5], which is thought to be the source of deformation for the quark core.

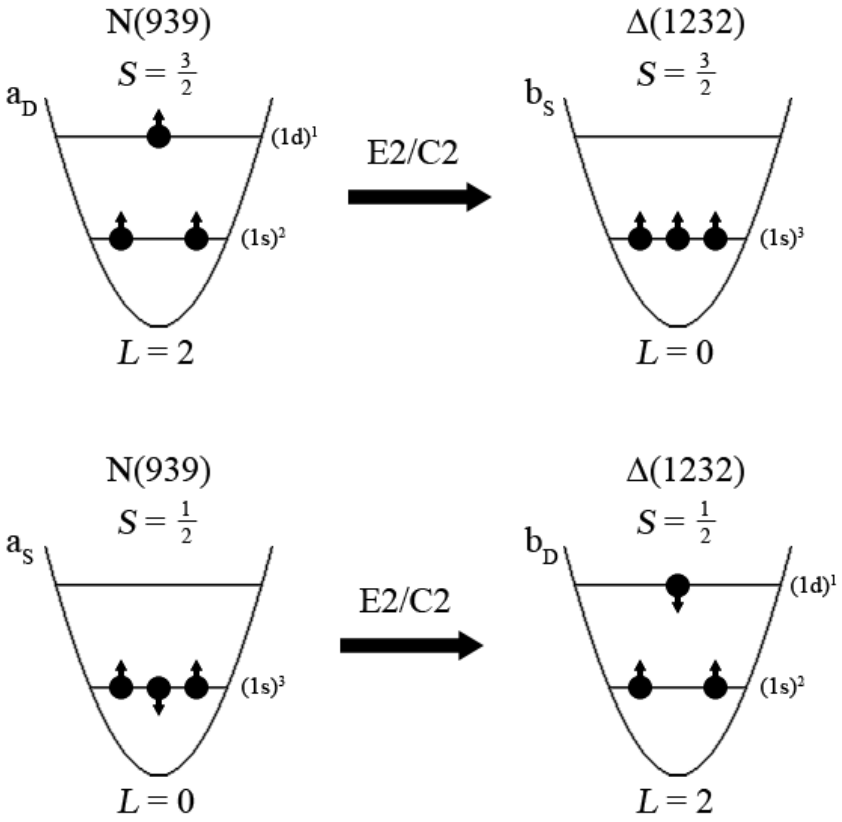

Figure 2: Quadrupole transitions.
Figures taken from Reference [3].

By measuring the strength of the quadrupole transitions, the strength of the $L = 2$ components of the nucleon's wave function can be indirectly measured, along with the nucleon's "deformation" (meaning its deviation from pure $L = 0$ spherical symmetry).

The transitions discussed so far are all one-body interactions. That is, the incoming photon only interacts with one quark (see Figure 3). The one-body quadrupole operator can be written as [3]:

$$\hat{Q}_{[1]} = \sqrt{\frac{16\pi}{5}} \sum_{i=1}^{3} e_i r_i^2 Y_0^2(\vec{r}_i) = \sum_i e_i (3z_i^2 - r_i^2)$$

Multiple-particle transitions are also possible (see Figure 4 on the next page). For example, a photon and a

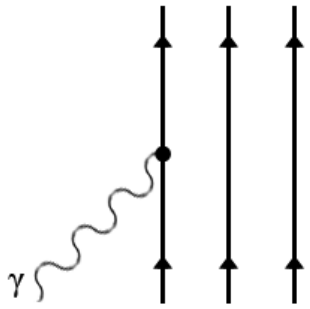

Figure 3: One-body transition.
Figure taken from Reference [3].

meson may interact with a quark at the same time, resulting in a quadrupole transition without a change in the orbital angular momentum of the quarks [3].

$$\hat{Q}_{[2]} = B\sum_{i\neq j=1}^{3} e_i(3\sigma_{iz}\sigma_{jz} - \vec{\sigma}_i \cdot \vec{\sigma}_j)$$

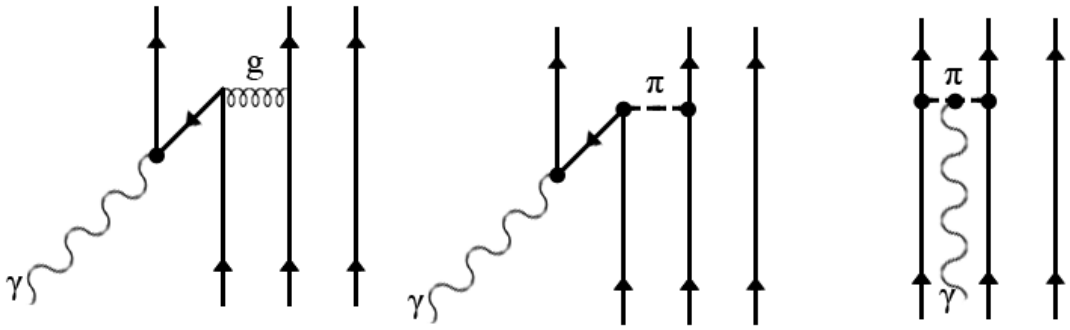

Figure 4: Two-body transitions.
Taken from Reference [3].

These mesons, which are predominantly pions, can be visualized as existing in a cloud surrounding the quark core. In this case, it can be imagined that it is not the quark core that is necessarily deformed, but this pion cloud, as shown in Figure 5.

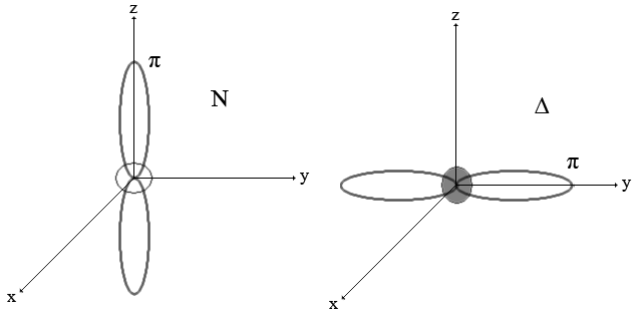

Figure 5: Pion cloud configurations. Figure taken from Reference [3].

Indeed, at low energies, the incoming photon may not have enough energy to interact with the quark core directly; instead, it interacts with the pion cloud, much in the same way that ultraviolet photons may interact with an atom's valence electrons while relatively higher energy

X-rays or gamma rays can penetrate deep into the electron cloud and interact with inner electrons or even the atom's nucleus.

This possibility could explain the discrepancy between CQM-based calculations and experimental results for the CMR in the region of low momentum transfer, since the CQM does not take the pion cloud into account, and it is the pion cloud with which low momentum photons are likely interacting [6].

3 Kinematics

In this experiment, the goal is to measure the Coulomb quadrupole transition amplitude. Since that amplitude can only be measured using virtual photons, the target protons will be excited using an electron beam. The electronic vertex is well known through quantum electrodynamics (QED), so no unnecessary complications will be added by using electrons for the proton excitation, in comparison to excitations using beams of nucleons or mesons, in which the strong interaction is involved [7].

The incoming electron has an energy E and a momentum $\vec{k}_i$. The interaction with the target proton causes the electron to scatter away with energy E' and momentum $\vec{k}_f$, at angle θ_e relative to the incoming electron's original direction, as shown in Figure 6. These quantities are used to set the physical position and momentum setting of the electron high resolution spectrometer (HRSe).

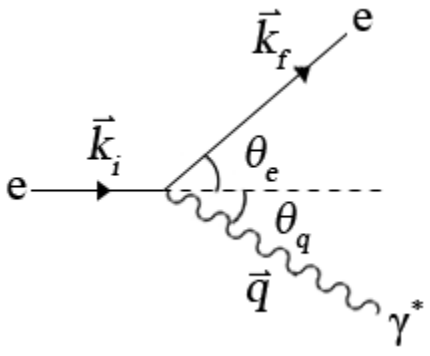

Figure 6: The electronic vertex.

The resulting change in the electron's energy and momentum is imparted to the virtual photon, which is described with energy ω and momentum $\vec{q}$, with an angle θ_q relative to the incoming electron's original direction. Combined, ω and $\vec{q}$ give a 4-momentum q, which is usually converted to $Q^2 = -q^2 = -\left(\omega^2 - \vec{q}^{\,2}\right)$. Q^2 is inversely related to the wavelength of the probing virtual photon and is usually referred to simply as the "momentum transfer".

The scattered electron angle θ_e is related to Q^2 through $Q^2 \approx 4EE'\sin^2\frac{\theta_e}{2}$, with the assumption that the electron's mass is much lower than its energy. This allows the value of Q^2 in the experiment to vary merely by changing the placement and momentum setting of the HRSe.

The virtual photon then interacts with the proton at the hadronic vertex, where the experimentally relevant interactions take place. If the energy transfer ω is tuned to approximately 300 MeV, the proton is then excited to a $\Delta(1232)$; but the Δ is short-lived and promptly decays, primarily to a nucleon and a pion, with nearly equal probabilities of p-π^0 and n-π^+ [8].

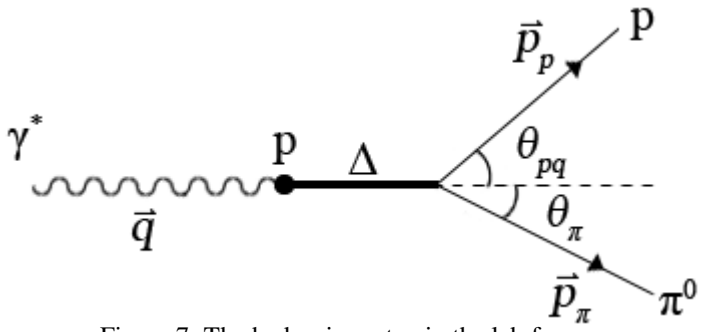

Figure 7: The hadronic vertex in the lab frame.

The experiment is specifically looking at the $p(e,e'p)\pi^0$ reaction, in which the proton target is initially stationary in the lab frame, and the recoil proton's momentum is given as $\vec{p}_p$, which makes an angle θ_{pq} with $\vec{q}$, as shown in Figure 7. This angle is important for setting the physical position of the proton/hadron high resolution spectrometer (HRSh).

The recoil pion is not directly observed, but its energy, E_π, and momentum, $\vec{p}_\pi$, in the lab frame, can be determined from missing mass calculations, in which the amount of energy and momentum missing in the final state, following detection of the scattered electron and recoil proton, is calculated using conservation of energy and momentum.

The vectors $\vec{k}_i$ and $\vec{k}_f$ form the scattering plane, while $\vec{p}_p$ and $\vec{p}_\pi$ form the reaction plane. The angle between these planes is ϕ_{pq} (seen in Figure 8 on the next page), the azimuthal angle in the lab frame, which plays an important role in extracting transition amplitude information.

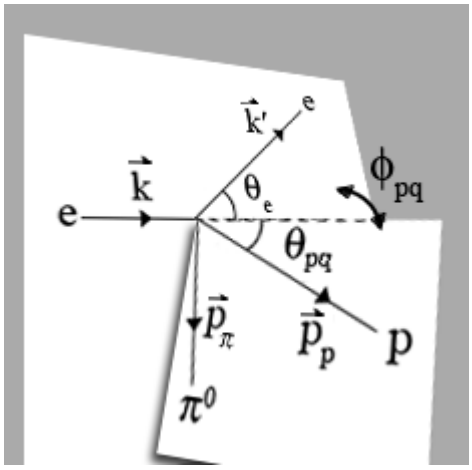

Figure 8: The scattering and reaction planes.

In the center of mass frame, the proton angle and the azimuthal angle are denoted θ^*_{pq} and ϕ^*_{pq}, and the target proton has a non-zero incoming momentum, as shown in Figure 9.

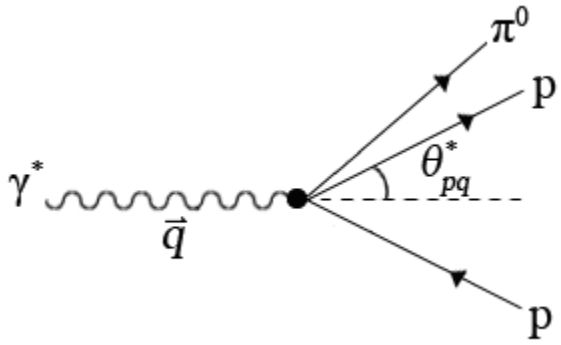

Figure 9: The center-of-mass hadronic vertex

4 Transition Amplitudes

Since the Δ cannot be detected directly, information about the transition amplitudes between the nucleon and the Δ must be collected from the Δ's decay products, the nucleon and the pion. However, since many possible reaction mechanisms could result in the production of a nucleon and a pion, it is necessary to differentiate between the different possibilities for these transition amplitudes.

The general notation of the (complex) transition amplitudes in which a nucleon and pion are produced is $X_{\ell\pm}^{I}$, where X denotes the type of excitation, I is the isospin of the excited intermediate state, ℓ is the orbital angular momentum of the system, and ± indicates whether the spin of the intermediate state is the result of the nucleon's spin being added to or subtracted from ℓ: $J = \ell \pm \frac{1}{2}$ [9].

The spin of the Δ, nucleon, and pion are $S = {}^{3}\!/_{2}$, ${}^{1}\!/_{2}$, and 0, respectively. This indicates that the decay of the Δ into the nucleon and pion must have an orbital angular momentum of either $\ell = 1$ or $\ell = 2$. Parity conservation further limits this to $\ell = 1$.

In the $p(e,e'p)\pi^0$ reaction, where the isospin of the Δ is $I = {}^{3}\!/_{2}$ and the ± must be +, the three multipoles of interest correspond to transition amplitudes as follows:

$$M1 \leftrightarrow M_{1+}^{3/2}$$
$$E2 \leftrightarrow E_{1+}^{3/2}$$
$$C2 \leftrightarrow S_{1+}^{3/2}$$

Occasionally in the literature, the scalar multipole, $S_{\ell\pm}$, is used interchangeably with the longitudinal multipole, $L_{\ell\pm}$, with the relation $\omega S_{\ell\pm} = |\vec{q}| L_{\ell\pm}$, where ω is the photon energy and $\vec{q}$ is the photon momentum [10].

In addition to the dominant M_{1+} and smaller resonant E_{1+} and S_{1+} amplitudes, there are a multitude of background amplitudes due to the other possible reaction mechanisms. Indeed, the primary difficulty in extracting the desired amplitudes from the data is that all the non-dominant amplitudes, both resonant and background, are at roughly the same magnitude [7].

Table 1 contains some of the amplitudes that may be present in the pion electroproduction reaction [11]. The resonant amplitudes are highlighted.

γN-Multipoles	Initial State		Excited State			Final State		πN-Multipoles
C, E, M	L_γ^π	s_N^π	J_R^π	$N^* I_{2I2J}\Delta$		s_N^π	I_π^π	$L_{\ell\pm}, E_{\ell\pm}, M_{\ell\pm}$
$C0$	0^+	$\frac{1}{2}^+$	$\frac{1}{2}^+$	P_{11}	P_{31}	$\frac{1}{2}^+$	1^+	L_{1-}
$C1, E1$	1^-	$\frac{1}{2}^+$	$\frac{1}{2}^-$	S_{11}	S_{31}	$\frac{1}{2}^+$	0^-	L_{0+}, E_{0+}
		$\frac{1}{2}^+$	$\frac{3}{2}^-$	D_{13}	D_{33}	$\frac{1}{2}^+$	2^-	L_{2-}, E_{2-}
$M1$	1^+	$\frac{1}{2}^+$	$\frac{1}{2}^+$	P_{11}	P_{31}	$\frac{1}{2}^+$	1^+	M_{1-}
		$\frac{1}{2}^+$	$\frac{3}{2}^+$	P_{13}	P_{33}	$\frac{1}{2}^+$	1^+	M_{1+}
$C2, E2$	2^+	$\frac{1}{2}^+$	$\frac{3}{2}^+$	P_{13}	P_{33}	$\frac{1}{2}^+$	1^+	L_{1+}, E_{1+}
		$\frac{1}{2}^+$	$\frac{5}{2}^+$	F_{15}	F_{35}	$\frac{1}{2}^+$	3^+	L_{3-}, E_{3-}
$M2$	2^-	$\frac{1}{2}^+$	$\frac{3}{2}^-$	D_{13}	D_{33}	$\frac{1}{2}^+$	2^-	M_{2-}
		$\frac{1}{2}^+$	$\frac{5}{2}^-$	D_{15}	D_{35}	$\frac{1}{2}^+$	2^-	M_{2+}

Table 1: Various transition amplitudes.

The S_{1+} and E_{1+} amplitudes act as interferences to the dominant M_{1+} amplitude [1]. For that reason, it is often convenient to refer to the strength of the smaller amplitudes with respect to the M_{1+} amplitude. These relative strengths are referred to as the electric-to-magnetic ratio (EMR) and the Coulomb-to-magnetic ratio (CMR), and are given as [12]:

$$EMR = R_{EM}^{3/2} = \mathrm{Re}\left(\frac{E_{1+}^{3/2}}{M_{1+}^{3/2}}\right) = \frac{\mathrm{Re}\left(E_{1+}^{*} M_{1+}\right)}{\left|M_{1+}\right|^2}$$

$$CMR = R_{CM}^{3/2} = \mathrm{Re}\left(\frac{S_{1+}^{3/2}}{M_{1+}^{3/2}}\right) = \frac{\mathrm{Re}\left(S_{1+}^{*} M_{1+}\right)}{\left|M_{1+}\right|^2}$$

5 Response Functions and Amplitude Extraction

The unpolarized differential cross section for the $p(e,e'p)\pi^0$ reaction is [13]:

$$\frac{d^5\sigma}{dk_f\, d\Omega_e\, d\Omega^*} = \Gamma_\gamma \frac{k}{q_0}\left[\varepsilon_S R_L + R_T + \sqrt{2\varepsilon_S(1+\varepsilon)}R_{LT}\sin\theta^*_{pq}\cos\phi^*_{pq} + \varepsilon R_{TT}\sin^2\theta^*_{pq}\cos 2\phi^*_{pq}\right],$$

where θ^*_{pq} and ϕ^*_{pq} have been previously defined,

$$\varepsilon = \left(1 + 2\frac{q^2}{Q^2}\tan^2\frac{\theta_e}{2}\right)^{-1}$$

is the transverse polarization of the virtual photon, and

$$\varepsilon_S = \frac{Q^2}{q^2}\varepsilon$$

is the longitudinal polarization of the virtual photon. Further,

$$\Gamma_\gamma = \frac{\alpha}{2\pi^2}\frac{k_f}{k_i}\frac{k_\gamma}{Q^2}\frac{1}{1-\varepsilon}$$

is the virtual photon flux for initial (final) electron momenta k_i (k_f), where

$$k_\gamma = \frac{W^2 - m_p^2}{2m_p}$$

is the laboratory energy a real photon would need to excite the same reaction, m_p is the proton mass, and W is the total reaction energy in the center-of-mass frame.

Finally,

$$k = \sqrt{\frac{W^2 + m_\pi^2 - m_p^2}{4W^2} - m_\pi^2}$$

is the center of mass proton momentum in the final state and

$$q_0 = \frac{W^2 - m_p^2}{2W}$$

is the center of mass momentum a real photon needs for the same transition.

R_L, R_T, R_{LT}, and R_{TT} are known as the unpolarized response functions. They can be thought of as independent partial cross sections and are directly related to the individual amplitudes, including the desired ones. For example, from Reference [11]:

$$R_L\sqrt{\frac{\omega_{cm}^2}{Q^2}} = \left|L_{0+}\right|^2 + 4\left|L_{1+}\right|^2 + \left|L_{1-}\right|^2 - 4\,\mathrm{Re}\left\{L_{1+}^* L_{1-}\right\} + 2\cos\theta\,\mathrm{Re}\left\{L_{0+}^*\left(4L_{1+} + L_{1-}\right)\right\} + 12\cos^2\theta\left(\left|L_{1+}\right|^2 + \mathrm{Re}\left\{L_{1+}^* L_{1-}\right\}\right)$$

$$R_T = \left|E_{0+}\right|^2 + \tfrac{1}{2}\left|2M_{1+} + M_{1-}\right|^2 + \tfrac{1}{2}\left|3E_{1+} - M_{1+} + M_{1-}\right|^2 + 2\cos\theta\,\mathrm{Re}\left\{E_{0+}^*\left(3E_{1+} + M_{1+} - M_{1-}\right)\right\}$$
$$+ \cos^2\theta\left(\left|3E_{1+} + M_{1+} - M_{1-}\right|^2 - \tfrac{1}{2}\left|2M_{1+} + M_{1-}\right|^2 - \tfrac{1}{2}\left|3E_{1+} - M_{1+} - M_{1-}\right|^2\right)$$

$$R_{LT}\sqrt{\frac{\omega_{cm}^2}{Q^2}} = -\sin\theta\,\mathrm{Re}\left\{L_{0+}^*\left(3E_{1+} - M_{1+} + M_{1-}\right) - \left(2L_{1+}^* - L_{1-}^*\right)E_{0+} + 6\cos\theta\left(L_{1+}^*\left(E_{1+} - M_{1+} + M_{1-}\right) + L_{1-}^* E_{1+}\right)\right\}$$

$$R_{TT} = 3\sin^2\theta\left(\tfrac{3}{2}\left|E_{1+}\right|^2 - \tfrac{1}{2}\left|M_{1+}\right|^2 - \mathrm{Re}\left\{E_{1+}^*\left(M_{1+} - M_{1-}\right) + M_{1+}^* M_{1-}\right\}\right)$$

There are several methods for extracting the amplitudes from the response functions. One, called the Truncated Multipole Expansion (TME) [14], simply assumes that any term without the dominant M_{1+} amplitude is small enough to safely ignore and remove from the equation.

With this method, the response functions approximate to

$$
\begin{aligned}
R_L &\approx 0 \\
R_T &\approx \tfrac{5}{2}\left|M_{1+}\right|^2 + 2\cos\theta\,\mathrm{Re}\left\{E_{0+}^{*}M_{1+}\right\} - \tfrac{3}{2}\cos^2\theta\left|M_{1+}\right|^2 \\
R_{LT} &\approx \sin\theta\,\mathrm{Re}\left\{L_{0+}^{*}M_{1+}\right\} - 6\cos\theta\left(L_{1+}^{*}M_{1+}\right) \\
R_{TT} &\approx -3\sin^2\theta\left(\tfrac{1}{2}\left|M_{1+}\right|^2 + \mathrm{Re}\left\{E_{1+}^{*}M_{1+} + M_{1+}^{*}M_{1-}\right\}\right)
\end{aligned}
$$

Since this experiment is concerned with the Coulomb transition amplitude $\left(S_{1+} = \frac{|\vec{q}|}{\omega}L_{1+}\right)$, there is specific interest in the R_{LT} response function. To extract the term with the S_{1+} in that response function, the equation can be manipulated using the azimuthal angle. By taking measurements at $\phi_{pq} = 0°$ and $\phi_{pq} = 180°$, with the same θ_{pq}, and combining the results and taking the difference, the sin θ term can be eliminated, leaving only the desired term.

Of course, this assumes a symmetry between the detector's acceptance for measurements at the two azimuthal angles. If such a symmetric acceptance can be achieved between the $\phi = 0°$ and $\phi = 180°$ measurements, then an experimental asymmetry (A_{LT}) can be formed which accesses the same combination of transition amplitudes (involving S_{1+}) as the R_{LT} response, but without the need for an overly accurate normalization of each measurement.

6 World Data

The first pion electroproduction experiments took place in 1969 at Harvard's Cambridge Electron Accelerator (CEA) [15]. It was during these experiments that the dominance of the M_{1+} transition amplitude was first discovered. Further experiments took place at the Deutsches Elektronen Synchrotron (DESY) between 1970 and 1972 [16] and the Daresbury Nuclear Physics Laboratory (NINA) in 1971 [17].

The current flurry of activity started in 1997, when pion electroproduction experiments at the Elektronen-Stretcher Anlage (ELSA) in Bonn produced rather unusual results [18]. That same year, pion photoproduction experiments were undertaken at Brookhaven's Laser Electron Gamma Source (LEGS) [19] and the Mainz Microtron (MAMI) [20]. Jefferson Lab's Hall C did

their own pion electroproduction experiments in 1998 [21], as did MIT-Bates in 2000 [22] and Mainz in 2001 [23].

In 2002, Jefferson Lab's Hall B, as part of the CEBAF Large Acceptance Spectrometer (CLAS) collaboration, ran a series of experiments with full angular acceptance [24], hoping to obtain a final, comprehensive, and complete measurement of the amplitudes in question. However, their experiments lacked polarization measurements of the recoil protons, which are necessary for such an undertaking. The missing polarization measurements were later taken by Jefferson Lab's Hall A in 2003 [7, 10, 12].

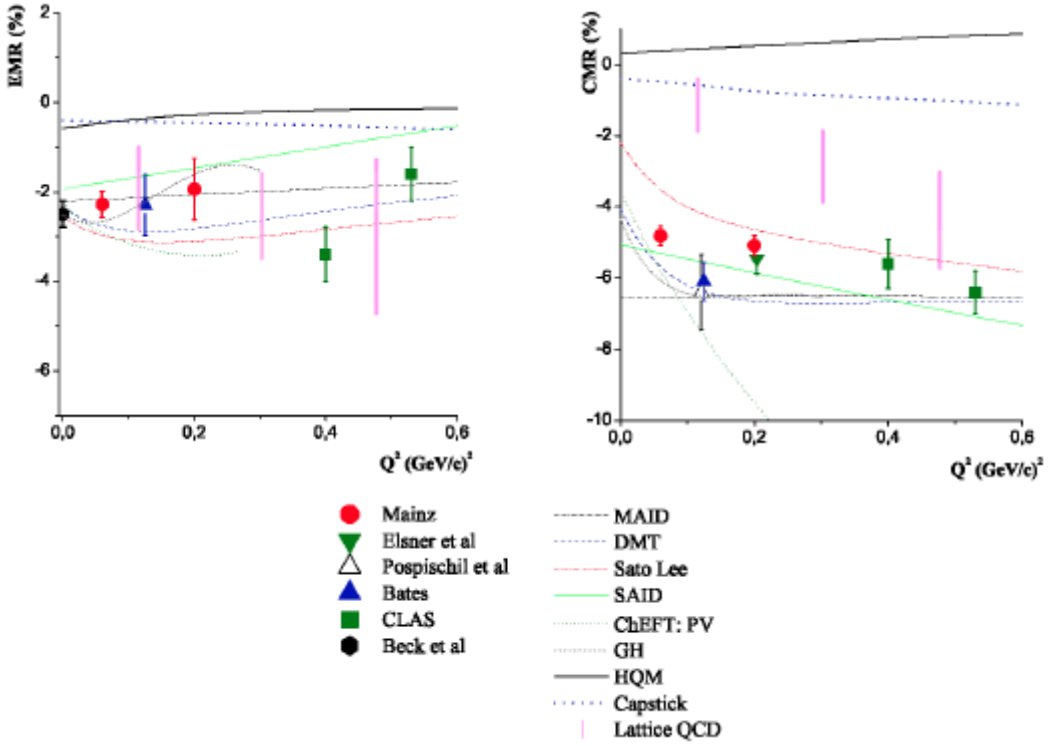

Figure 10: The EMR and CMR world data [1].

In 2004, further pion electroproduction measurements were made at MIT-Bates, utilizing the OOPS detector [25]. In 2005 [26] and 2006 [27x-28x], a series of experiments at Mainz explored the area around $Q^2 = 0.2$ (GeV/c)^2 [26x-27x] as well as getting the then-lowest measurements at $Q^2 = 0.060$ (GeV/c)^2 [28].

Altogether, these experiments produced the world data on the EMR and CMR, displayed in Figure 10, conclusively proving that the nucleon is indeed deformed. However, while the many pion electroproduction experiments vary over a wide range of Q^2 values, it is felt that more

CMR data could be collected in the low Q^2 region (shown in Figure 11), where the pion cloud, rather than the quark core, is expected to have a significant influence on the CMR values [1]. Indeed, the primary reason for this experiment is to further explore that region.

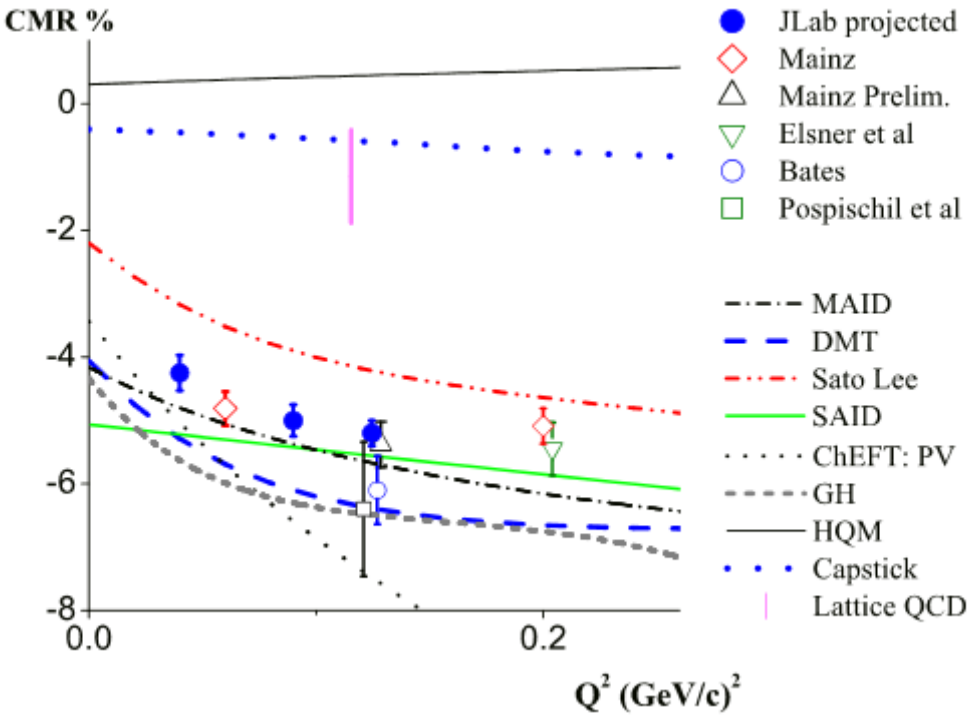

Figure 11: The CMR world data for low Q^2 [1].

The lowest Q^2 value for which the CMR has been measured is $Q^2 = 0.060$ (GeV/c)^2 [23]. This experiment will go lower, to $Q^2 = 0.040$ (GeV/c)^2, a feat made possible by the unique configuration in Jefferson Lab's Hall A, where the positioning of HRSe can reach as low as $\theta_e = 12.5°$ [29].

Further, the CMR data collected in the vicinity of $Q^2 = 0.125$ (GeV/c)^2 has shown a curious dip. This experiment will take high precision measurements at that value to help validate and clarify the previous measurements.

Data will also be taken at $Q^2 = 0.090$ (GeV/c)^2 to bridge previous measurements, specifically between the aforementioned $Q^2 = 0.060$ (GeV/c)^2 and $Q^2 = 0.125$ (GeV/c)^2.

7 Models

As mentioned earlier, there are several methods for extracting the amplitudes from the response functions. Another method is known as the Model Dependent Extraction (MDE) [14], where a theoretical model is fit to available data and used to extract the wanted transition amplitudes.

Two commonly used models are both phenomenological, MAID [30] and SAID [31]. Both models are computational, using scattering amplitudes with parameterizations, but MAID is derived from the Mainz Unitary Isobar Model and SAID is derived from a phase shift analysis of the world data.

One dynamical model commonly used is DMT. It has the same resonance terms as MAID, but different background terms [32].

There are also models based more directly on the underlying QCD, such as chiral effective field theory [33] and lattice QCD [34]. Lattice QCD is of particular interest, as it attempts to take QCD to the lower energy regions where traditional perturbation methods are no longer valid. However, this has met with little success in the area of understanding nucleon deformation, since the theoretical predictions are far from the experiment data for the EMR and CMR.

However, this failure may be explained by a dynamical model created by Sato and Lee [6]. They propose to theoretically treat the nucleon as a "bare" quark core surrounded by a pion cloud. In Figure 12, this can be seen, where the solid lines show the transition amplitudes for the full calculation (quark core plus pion cloud), while the dashed lines show the amplitudes for the quark core contribution only. With this approach, they can compare the "full" nucleon to the experimental data while comparing the "bare" core to lattice QCD results, hopefully finding a way to link QCD to this low energy region.

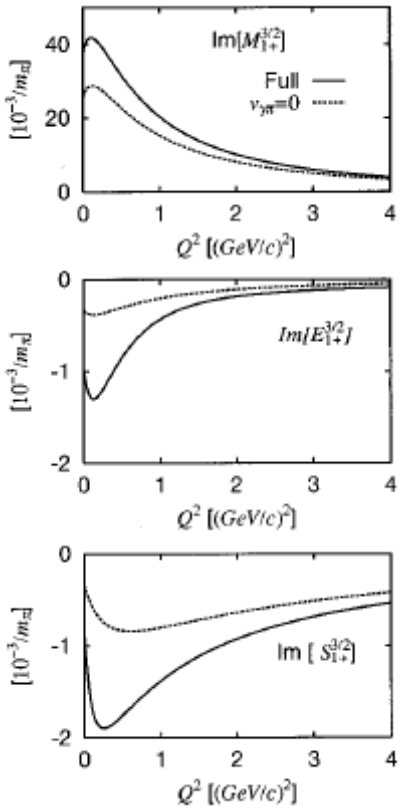

Figure 12: The Sato-Lee model predictions [6].

8 The Experiment

The experiment E08-010 will take place in Hall A (shown in Figure 13) at the Thomas Jefferson National Accelerator Facility (Jefferson Lab) in Newport News, Virginia, in April of 2011. An electron beam generated with a current of 75 μA and an energy of 1115 MeV will be directed at a 6 cm liquid hydrogen target [1]. The recoil particles will be detected by Hall A's two high resolution spectrometers, one for the electrons and one for the protons.

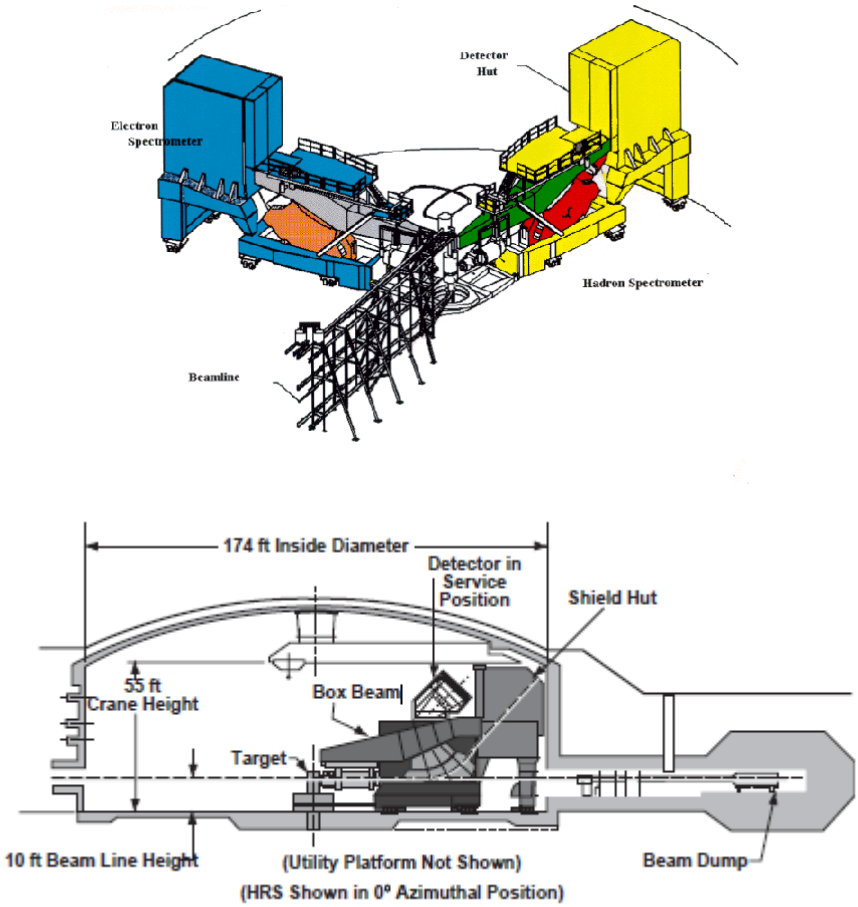

Figure 13: Jefferson Lab's Hall A [25, 31].

8.1 Continuous Electron Beam Accelerator Facility

The electron beam will be produced at the Continuous Electron Beam Accelerator Facility (CEBAF) (shown in Figure 14 on the next page), one of two accelerator facilities at Jefferson Lab. The beam is produced by illuminating a gallium-arsenide (GaAs) cathode with a 1497 MHz gain-switched 780 nm diode laser [29].

This beam is then injected into the accelerator, which consists of two linear accelerators (linacs) and two magnetic recirculation arcs. As the names suggest, the beam is accelerated in the linacs before entering the arcs which curve the beam so that it can be recirculated into the opposite linac. The beam starts in the north linac and can be recirculated a number of times before exiting after the south linac, where it can then be directed to the three halls simultaneously.

The linacs themselves consist of twenty superconducting cryomodules and can reach a maximum energy of 5.7 GeV, after five loops.

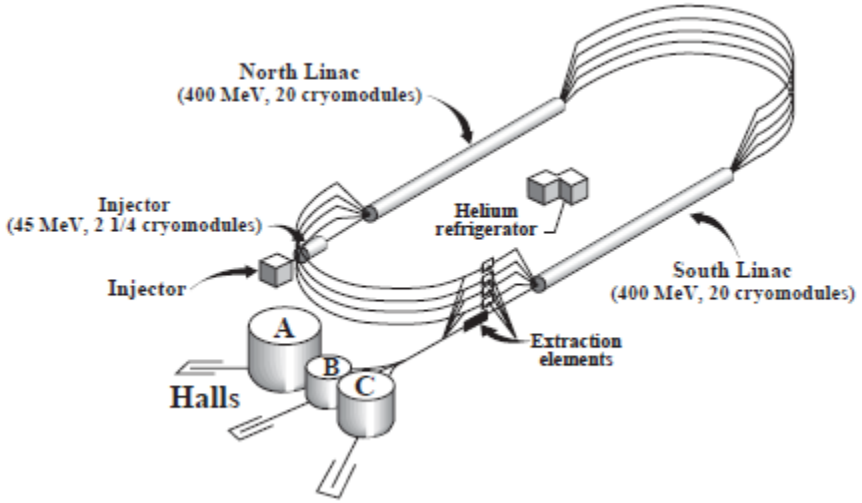

Figure 14: The Continuous Electron Beam Accelerator Facility [29].

8.2 Liquid Hydrogen Target

The Hall A cryogenic target system consists of a scattering chamber and a target ladder [29].

The scattering chamber has several ports for vacuum pumps, visual inspection, and electrical feedthroughs, as well as beam entrance and exit ports, ensuring that the beam only interacts with the target.

The target ladder contains three cryogenic loops: a liquid hydrogen loop (LH_2), a liquid deuterium loop (LD_2), and a gaseous helium loop. These loops can be manipulated remotely, allowing new targets to move into position without opening the hall. There are also "dummy" targets and solid targets for calibration and spectrometer pointing measurements.

8.3 High Resolution Spectrometers

The two high resolution spectrometers are the central pieces of Hall A. They both contain four superconducting magnets in a quadrupole-quadrupole-dipole-quadrupole (QQDQ) configuration [29], designed to direct incoming charged particles to the detectors. The design was optimized for angular and momentum acceptance, position and angle resolution, target acceptance, and angular range.

While both spectrometers can be configured to detect a variety of particles, in this experiment one will be used to detect the scattered electrons (designated here as HRSe), and one for the recoil protons (designated here as HRSh). The basic hardware configuration for both spectrometers is virtually identical.

The basic detector package consists of two vertical drift chambers (VDCs), two scintillators, an aerogel Cerenkov detector, a gas Cerenkov detector, and a set of lead-glass shower counters [29]. Depending on the particular experiment, other components can be added or removed. For example, if the polarization of the recoil proton is needed, the Focal Plane Polarimeter (FPP) may be added to the HRSh, as seen in Figure 15.

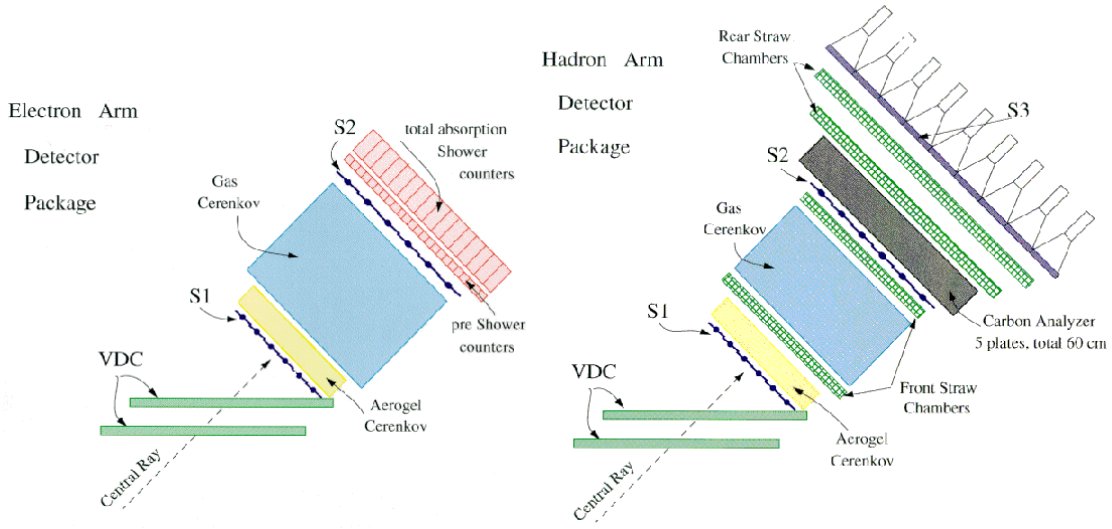

Figure 15: The High Resolution Spectrometer Detector Packages [32, 33]

The scintillators are used for timing information and triggering the data acquisition software (DAQ), the VDCs allow for particle tracking, and the Cerenkov detectors and the lead-glass shower counters are used for particle identification, which is important in this experiment, as the pions will need to be separated from the protons.

Table 2 lists the operating specifications for the high resolution spectrometers.

Momentum Range	0.3 - 4.0 GeV/*c*
Configuration	QQDQ
Bend Angle	45°
Optical Length	23.4 m
Momentum Acceptance	± 4.5%
Dispersion (D)	12.4 cm/%
Radial Linear Magnification (M)	2.5
D/M	5
Momentum Resolution (FWHM)	1×10^{-4}
Angular Acceptance Horizontal Vertical	 ± 28 mr ± 60 mr
Solid Angle (rectangular approximation) (elliptical approximation)	 6.7 msr 5.3 msr
Angular Resolution Horizontal Vertical	 0.6 mr 2.0 mr
Transverse Length Acceptance Transverse Position Resolution (FWHM)	± 5 cm 1.5 mm
Spectrometer Angle Determination Accuracy	0.1 mr

Table 2: The High Resolution Spectrometer Information [35].

8.4 Settings

Over the course of the experiment, there will be 14 different position configurations of the two high resolution spectrometers. As the Q^2 values are dependent on the energy and angle of the scattered electrons, the HRSe will be physically moved to accommodate the different Q^2 values in the experiment. The HRSh will be moved for each configuration.

A complete list of the 14 configuration settings are shown in Table 3, including the lab frame angles of both spectrometers, the spectrometer's central momentum acceptance values, and the calculated time to collect data at those settings [1].

Q^2 (GeV/c)^2	W (MeV)	θ^*_{pq} °	θ_e°	P'_e (MeV/c)	θ_p°	P'_p (MeV/c)	Time (hrs)
0.040	1221	0	12.52	767.99	24.50	547.54	1.5
0.040	1221	30	12.52	767.99	12.52	528.12	2
0.040	1221	30	12.52	767.99	36.48	528.12	3.5
0.040	1260	0	12.96	716.42	21.08	614.44	1.5
0.090	1230	0	19.14	729.96	29.37	627.91	1.5
0.090	1230	40	19.14	729.96	14.99	589.08	3
0.090	1230	40	19.14	729.96	43.74	589.08	4.5
0.125	1232	0	22.94	708.69	30.86	672.56	3.5
0.125	1232	30	22.94	708.69	20.68	649.23	7
0.125	1232	30	22.94	708.69	41.03	649.23	7
0.125	1232	55	22.94	708.69	12.52	596.43	3.5
0.125	1232	55	22.94	708.69	49.19	596.43	3.5
0.125	1170	0	21.74	788.05	37.31	575.57	3
0.125	1200	0	22.29	750.16	34.06	622.63	2
Configuration changes							17
Calibrations							8
			Total:				72

Table 3: The experimental settings.

With the requested beam time, the settings should result in a better than ±1% statistical uncertainty and a ±3% systematic uncertainty for the cross sections in each analysis bin [1]. Further, a conservative estimate of 20% dead time and a 99% detection efficiency have been assumed in the setting calculations.

To extract the resonant amplitudes from the background, a Model Dependent Extraction will be used, utilizing the fact that there are several models available (MAID, SAID, DMT,

Sato-Lee) to minimize model dependence of the extraction. The final CMR uncertainties should be better than 0.28%, 0.25%, and 0.20% for Q^2 = 0.040 (GeV/c)^2, Q^2 = 0.090 (GeV/c)^2, and Q^2 = 0.125 (GeV/c)^2, respectively [1].

9 Conclusions

This experiment is an important step forward in understanding why the proton has the internal structure it has. Additionally, the CMR values at these Q^2 settings could help theoretical models like Sato and Lee's better understand how the pion cloud contributes to nucleon deformation and how QCD plays a role in subatomic physics in the low energy regime.

References

[1] N. Sparveris, S. Gilad, D.W. Higinbotham, A. Sarty (Spokespersons), Measurement of the Coulomb quadrupole amplitude in the $\gamma^*p \rightarrow \Delta(1232)$ in the low momentum transfer region. Jefferson Lab Hall A Proposal E08-010, 14p, 2007. http://www.jlab.org/exp_prog/proposals/08/PR-08-010.pdf

[2] S.L. Glashow, Physica **A 96**, 27 (1979)

[3] A.J. Buchmann and E.M. Henley, Phys. Rev. **C63**, 015202 (2000)

[4] C. Mistretta *et al.*, Phys. Rev. **184**, 1487 (1969)

[5] N. Isgur, G. Karl, and R. Koniuk, Phys. Rev. **D 25**, 2394 (1982)

[6] T. Sato and T.-S.H. Lee, Phys. Rev. **C63**, 055201 (2001)

[7] R. Roché, Ph.D. thesis, Florida State University (2003)

[8] C. Amsler *et al.*, Phys. Lett. **B 667**, 1 (2008)

[9] J. Glister, Ph.D. thesis, Dalhousie University (2009)

[10] Z.Chai, Ph.D. thesis, Massachusetts Institute of Technology (2003)

[11] D. Dreschel and L. Tiator, J. Phys. **G18**, 449 (1992)

[12] J.J. Kelly, *et al.*, Phys Rev **C75**, 025201 (2007)

[13] J.J. Kelly, Phys Rev **C72**, 048201 (2005)

[14] E. Stiliaris and C.N. Papanicolas, AIP Conf. Proc. **904**, 257 (2007)

[15] A. de Rujula, H. Georgi and S.L. Glashow *et al.*, Phys Rev **D12**, 147 (1975)

[16] W. Albrecht *et al.*, Nucl. Phys. **B25**, 1 (1970); Nucl. Phys. **B27**, 615 (1971); J.C. Alder *et al.*, Nucl. Phys. **B46**, 573 (1972)

[17] R. Siddel *et al.*, Nucl. Phys. **B35**, 93 (1971)

[18] F. Kalleicher *et al.*, Z. Phys. **A359**, 201 (1997)

[19] G. Blanpied *et al.*, Phys. Rev. Lett. **79**, 4337 (1997)

[20] R. Beck *et al.*, Phys. Rev. Lett. **78**, 606 (1997)

[21] V. V. Frolov *et al*., Phys. Rev. Lett. **82**, 45, (1999)

[22] C. Mertz *et al.*, Phys. Rev. Lett. **86**, 2963 (2001)

[23] Th. Pospischil *et al.*, Phys. Rev. Lett. **86**, 2959 (2001)

[24] K. Joo *et al.*, Phys. Rev. Lett. **88**, 122001 (2002)

[25] N.F. Sparveris *et al.*, Phys. Rev. Lett. **94**, 022003 (2005)

[26] D. Elsner *et al.*, Eur. Phys. J. **A 27,** 91-97 (2006)

[27] N.F. Sparveris *et al.*, Phys. Lett. **B 651**, 102 (2007)

[28] S. Stave *et al.*, Eur. Phys. J. **A 30**, 471 (2006)

[29] J. Alcron *et al.*, Nucl. Instrum. Methods **A 522**, 294 (2004)

[30] D. Dreschel *et al.*, Nucl. Phys. **A645**, 145 (1999)

[31] R.A. Arndt, I.I. Strakovsky, R. L. Workman, Phys. Rev. **C53**, 430 (1996)

[32] S.S. Kamalov and S.N. Yang, Phys. Rev. Lett. **83**, 4494 (1999)

[33] V. Pascalutsa and M. Vanderhaegen *et al*., Phys. Rev. Lett. **95**, 232001 (2005); Phys Rev. **D73**, 034003 (2006)

[34] C. Alexandrou *et al.*, Phys. Rev. D69, 114506 (2004); Phys. Rev. Lett. **94**, 021601 (2005)

[35] http://hallaweb.jlab.org/equipment/high_resol.html

[36] http://hallaweb.jlab.org/equipment/detectors/det_electrons.html

[37] http://hallaweb.jlab.org/equipment/detectors/det_hadron.html